PAPER

CrossMark
click for updates

Fluorescein hydrazone-based supramolecular architectures, molecular recognition, sequential logic operation and cell imaging†

Kamini Tripathi,[a] Abhishek Rai,[a] Amarish Kumar Yadav,[b] Saripella Srikrishna,[b] Niraj Kumari*[a] and Lallan Mishra*[a]

A fluorescein hydrazone (**FDNS**) is prepared by the coupling of fluorescein hydrazide with 3,5-dinitrosalicylaldehyde. It is well characterized using spectroscopic (IR, UV-visible, ^{1}H, ^{13}C NMR, ESI-MS) techniques and X-ray crystallography. **FDNS** is embedded with several H-bonding domains which provide interesting intra and inter molecular H-bonded networks. Its crystal packing along the *b* crystallographic axis using H-bonding interactions provides a fascinating helical structure. It detects Cu^{2+} ions selectively over many relevant ions and displays a novel peak at $\lambda_{max} = 495$ nm. The significant enhancement in its fluorescence is observed with a peak at $\lambda_{em} = 517$ nm on addition of Hg^{2+} ions, which is quenched upon the addition of S^{2-} ions. The sensing of Hg^{2+} ions by **FDNS** follow a hydrolysis pathway whereas the binding of Cu^{2+} ions with **FDNS** provides a colour change. The addition of a solution of tetrabutylammoniumcyanide in methanol to a corresponding solution of **FDNS** caused a turn to a green colour immediately. But on keeping the solution at room temperature for 72 h, red coloured crystals are obtained. The crystals were authenticated by X-ray crystallography. It was found to be a new compound **FKCN** in which a tetrabutylammonium cation is co-crystallized with deprotonated **FDNS**. Its supramolecular assembly *via* H-bonding provides an interesting ladder type architecture. **FDNS** displays chronological logic gate-based detection of several ions (Cu^{2+}, Hg^{2+}, EDTA, and S^{2-}) at ppm levels. The real sample analysis, live cell imaging and portable paper strip based detection of Cu^{2+} and Hg^{2+} ions *via* an obvious colour change endows **FDNS** with great economic significance in recognition processes.

1. Introduction

The design and synthesis of adaptable molecules which can detect multiple analytes is of great significance as they provide the understanding of molecular interactions in recognition processes. Among several designed frameworks, fluorescein derivatives have extensively been exploited as structural scaffolds for optical probes due to their brilliant photophysical properties, such as longer absorption, emission wavelengths and large absorption coefficients.[1–6] The spirolactam ring of fluorescein derivatives is a typical model for the design of molecular switches. Few interesting studies of the sensors for

multiple-analytes have been reported earlier.[7–14] In the area of molecular recognition, simultaneous detection of multiple ions has been the centre of attraction. In this context, toxicity of Hg^{2+} ions owes to its easy crossing of cell membrane barrier and warrants a simple design of its receptor. On the other hand, Cu^{2+} plays diverse physiological activities and its excess or scarcity leads Alzheimer's, Wilson's and Parkinson's diseases.[15,16] Among the anions, cyanide and sulphide are considered very important toxicants and they are generated from several industrial sources. Therefore, a rapid method to detect multiple ions with a single optical probe accessible in environmental and biological systems is in great demand.[17,18] The design of a logic device for the conversion of chemically encoded information into the optical signals has emerged as a demanding area of research.[19,20]

In this context, it has also been observed that such designed molecular systems can display several types of supramolecular architectures if they are embedded specially with H donors and H-acceptor components. In fact, the area of crystal engineering has been enriched with several interesting organic compounds with stunning display of supramolecular architectures. The multiple hydroxyl group containing ligands have proven as

aDepartment of Chemistry, Institute of Science, Banaras Hindu University, Varanasi, India. E-mail: nirajchem@gmail.com; lmishrabhu@yahoo.co.in; Fax: +91-542-2368127; Tel: +91-542-6702449

bDepartment of Biochemistry, Institute of Science, Banaras Hindu University, Varanasi, India

Paper

perfect candidate as they know how to act as hydrogen donors and acceptors. The recognition at molecular level involves several non covalent interactions like hydrogen bonding, CH–π interaction as well as π–π stacking together with hydrophobic forces.[21] The fluorescein dye and its derivatives richly embedded with several H-bonding domains are considered appropriate organic compounds for the construction of different type of supramolecular structures. In the present context, 3,5-dini-trosalicylaldehyde was selected as a coupling component as it was anticipated to impart the fluorescence enhancement of overall framework as compared to earlier used 5-nitrosalicylaldehyde.[22]

Thus, based on the above precedence, fluorescein hydrazide condensed with 3,5-dinitrosalicylaldehyde provided the desired compound (**FDNS**) which is characterized using full battery of physico chemical techniques and X-ray crystallography. As anticipated, it was empowered with the discriminatory recognition of Cu^{2+} and Hg^{2+} ions and it's **FDNS**–Cu^{2+} adduct acted as secondary sensor of CN^- ions. The H-bonding components embedded on its skeleton, enable the formation of intra and intermolecular interactions. These interactions lead interesting supramolecular assembly and provide helical structure. It also acts as a module for computing sequential logic operations.

2. Experimental

2.1. Materials and methods

All chemicals were obtained from industrial sources. The CE-440 Elemental analyzer is used for elemental analyses of C, H, and N. Varian 3300 FT-IR and Shimadzu UV-1601 were used for recording their IR and UV-visible spectra, respectively. ^1H (500 MHz) and ^{13}C (100 MHz) NMR spectra were recorded via JEOL AL500 FT-NMR spectrometer. Perkin Elmer Fluorescence spectrophotometer is used for the measurement of fluorescence spectrum in aqueous : MeOH (8 : 2, v/v, HEPES buffer (1 mM), pH 7.4) at room temperature. ESI-MS was obtained using a mass spectrophotometer of made WATERS Q-TOF Premier-HAB213. The yellow crystals of **FDNS** were obtained through slow evaporation of its solution in DMSO at room temperature. X-ray diffraction data were collected using Oxford diffraction XCALIBUR-EOS diffractometer with monochromated Mo K_α radiation ($\lambda = 0.71073$ Å). The data were solved by using SHELXS-97 Program[23] whereas they were refined by full matrix least squares SHELXL-97.[24]

2.2. Synthesis

The fluorescein hydrazone (**FDNS**) is synthesized by refluxing fluorescein hydrazide (0.345 g, 1 mmol) and 3,5-dini-trosalicylaldehyde (0.21 g, 1.1 mmol) in absolute ethanol (20 mL), on water bath for 8 h, under N_2 atmosphere. A yellow precipitate was obtained, which was filtered and washed with ethanol to give desired fluorescein hydrazone (**FDNS**) in 75% yields (Scheme 1). The yellow colour crystals of **FDNS** were developed by the slow evaporation of a solution of **FDNS** in DMSO at room temperature. Mp > 200 °C; FT-IR (KBr, cm^{-1}): 3333 (OH), 3082 (Ar-H), 1696 (C=O), 1609 (C=N), 1262 (C–O); ^1H NMR (500 MHz, DMSO-d$_6$): δ 9.93 (s, 1H, OH), 9.03(s, CH=
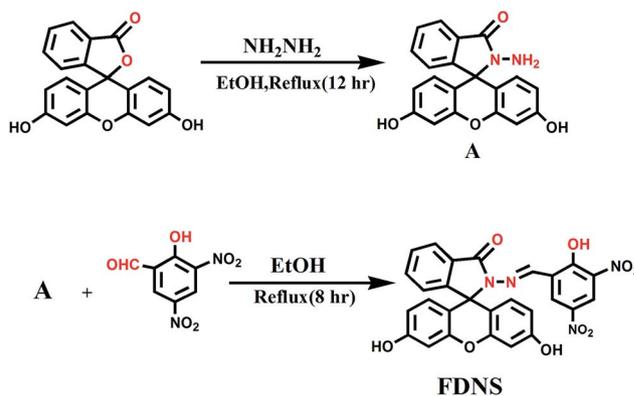
Scheme 1 Synthesis of **FDNS**.

N, 1H), 8.64 (bs, 1H), 8.54 (bs, 1H), 7.97 (d, 1H, J = 8.0 Hz), 7.63 (m, 2H), 7.14 (d, 2H, J = 7.5 Hz), 6.69 (s, 2H), 6.55 (d, 2H, J = 8.5), 6.47 (d, 2H, J = 10.5); ^{13}C NMR (100 MHz, DMSO-d$_6$): 182.35, 174.19, 168.47, 165.67, 164.05, 158.74, 153.99, 147.35, 152.27, 145.40, 138.41, 135.20, 130.69, 123.69, 122.90, 113.10, 110.20, 104.10, 98.31, 65.01, 51.69; EI-MS m/z 541.1003; elemental analysis (calcd%) for $C_{27}H_{16}N_4O_9$: C, 60.00; H, 2.98; N, 10.37; found C, 59.91; H, 2.90; N, 10.17.

FKCN was synthesized by the addition of excess solution of tetrabutylammoniumcyanide to a solution of **FDNS** in methanol containing copper nitrate solution in methanol. Red colour crystals suitable for X-ray measurement were obtained. Mp > 200 °C; FT-IR (KBr, cm^{-1}): 3303 (OH), 2963–2873 (aliphatic-H), 1702 (C=O), 1602 (C=N), 1263 (C–O); ^1H NMR (500 MHz, DMSO-d$_6$): δ 9.91 (s, 1H, OH), 8.81 (s, CH=N, 1H), 8.47 (s, 1H, Ar), 8.14 (s, 1H, Ar), 7.88 (s, 1H, Ar), 7.54 (m, 2H, Ar), 7.05 (d, 1H, Ar), 6.64 (s, 1H, Ar), 6.47 (m, 2H, Ar), 6.43 (m, 2H, Ar), 3.16 (m, 8H, CH$_2$), 1.55 (m, 8H, CH$_2$), 1.31 (m, 8H, CH$_2$), 0.92 (m, 12H, CH$_3$); ^{13}C NMR (DMSO-d$_6$): 194.61, 163.64, 158.52, 151.90, 151.28, 145.04, 138.00, 133.83, 128.48, 127.61, 122.76, 112.36, 109.83, 102.70, 64.84, 23.06, 19.21, 13.49.

2.3. Determination of binding constants

The binding constant of the formation of Cu^{2+}/Hg^{2+} complexes were evaluated using Benesi–Hildebrand (B–H) plot (eqn (1)).[25]

$$1/(A - A_0) = 1/\{K(A_{max} - A_0)C\} + 1/(A_{max} - A_0) \qquad (1)$$

The symbol A_0 and A corresponds to absorbance of **FDNS** at $\lambda_{max} = 554$ nm and absorbance observed at a particular concentration of the metal ion (C), whereas A_{max} is obtained at $\lambda_{max} = 495$ nm, respectively. The apparent binding constant K (M^{-1}), is calculated from the slope of the linear plot.

2.4. Method for spectroscopic investigation

The stock solution of **FDNS** (1×10^{-5} M) was prepared in aqueous : MeOH (8 : 2 v/v) solution and solutions of metal ions (1×10^{-2} M) were prepared using their nitrate salts in water. A solution of tetrabutylammoniumcyanide (1×10^{-2} M) was

prepared in distilled water. Before UV-visible and fluorescence measurements all samples were equilibrated for 1 min.

2.5. Real sample analysis of Cu^{2+} and Hg^{2+} ions

The three water samples (river, pond and lake) were used to prepare the required samples after filtration. All the water samples (3.0 mL) were spiked independently with different concentrations (0–10 μM) of Cu^{2+} and Hg^{2+} ions followed by the addition of **FDNS** (10 μM) to corresponding solutions.

2.6. Detection limit

The limit of detection was evaluated by means of UV-visible and florescence titrations. The absorption and emission spectrum of **FDNS** was measured at 10 times, and the standard deviation of blank measurement was achieved. The graph of the UV-visible absorbance at $\lambda_{max} = 495$ nm and florescence $\lambda_{max} = 517$ nm was plotted repetitively *vs.* the concentration of Cu^{2+} and Hg^{2+} ions to get the slope. The limit of detection was calculated using equation LOD = $3\sigma/k$ where σ is standard deviation of blank measurement.[26]

2.7. Cell culture, compound treatments and fluorescence imaging

Cervical cancer cell lines (ME-180) obtained from National Centre for Cell Science (NCCS), Pune, India, were cultured in Dulbecco's modified Eagle's medium (DMEM, HiMedia) supplemented with 10% FBS and 1× antibiotic cocktail in CO_2 incubator at 37 °C. For cell imaging experiment, the cultured cells were washed with 1× PBS followed by trypsinization for 2 min and collected in Eppendorf tube. Cells were incubated with **FDNS** (10 μM) for 45 min at room temperature and in other set, cells were initially treated with **FDNS** (10 μM) for 30 min followed by addition of Hg^{2+} (50 μM) for 15 min, while control set was treated with solvent alone (methanol and water in 1 : 9 ratio). After incubation, cells were centrifuged at 2000 rpm for 1 min and washed twice with 1× PBS for 2 min each. Cells were mounted in 1× PBS and images were captured with Nikon Ni-U fluorescence microscope using FITC filter-Ex-465-496, DM 505, BA 515-555. Fluorescence intensity was measured using Nikon-NIS-element BR software.

3. Results and discussion

The compound **FDNS** is characterized by IR, ^{1}H NMR, ^{13}C NMR, ESI-MS spectral data and elemental analysis. Its structure was further legitimate by X-ray crystallography and molecular structure (ORTEP diagram) is depicted in Fig. 1.

IR spectrum of **FDNS** displays a distinct peak at ν 1609 cm^{-1} assigned to ν(HC=N) stretching vibration (Fig. S1†). Its ^{1}H and ^{13}C NMR spectrum are shown in Fig. S2 and S3† respectively and supports the existence of CH=N group at δ 9.04 ppm in solution. ESI-MS also supports the formation of **FDNS** with the peak at *m/z* 541.1003 corresponding to [**FDNS** + H]$^+$ (Fig. S4†). Appearance of a peak at δ 65.01 ppm for spiro carbon in its ^{13}C NMR spectrum supported the presence of spiro-cyclic ring in its structure.[27] The UV-visible spectrum of **FDNS** showed peak at
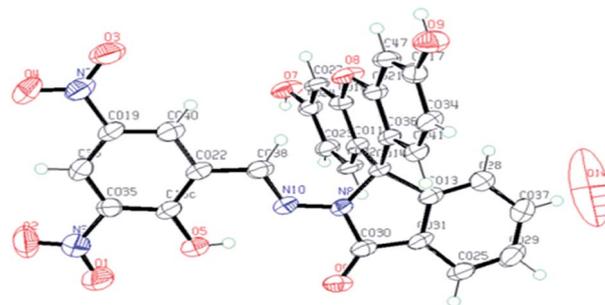

Fig. 1 Molecular structure (ORTEP diagram) of **FDNS** at 40% probability level.

$\lambda_{max} = 401$ nm ($\varepsilon = 25\,800$ M^{-1} cm^{-1}) designated to intramolecular charge transfer transition. Some structural parameters are presented in Table S1† whereas the selected bond distances (Å) and bond angles (deg) were presented in Table S2.† The selected parameters for weak interactions are listed as Table S3.† It is quite interesting to visualise the molecule **FDNS** as a typical paddle-wheel type structure, having a dihedral angle of 85.62° between two coordination planes (Fig. 2a). An intramolecular hydrogen bond formation between O5–H006⋯N10 could be seen as depicted in Fig. 2b. It provides a six-membered pseudo-ring consisting of N10–C038–C032–C16C–O5–H006 system. The bond distance between H006⋯N10 is found as 1.814 Å with a bond angle of 147.17° between O5–H006⋯N10. The molecule is associated through two type of intermolecular H-bond formation (Fig. 2c). One bond is formed between –OH (O9–H007) of one molecule and one of the nitro groups (O2–N3–O1) of another molecule of **FDNS**. The second intermolecular H-bond is formed between carbonyl group (C030–O6) of one **FDNS**
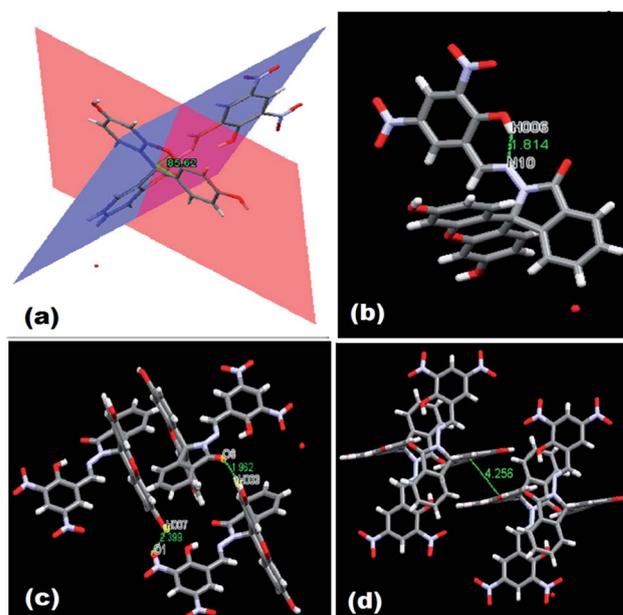

Fig. 2 Different structures of **FDNS** (a) paddle wheel structure (b) intra molecular H-bonding, (c) inter molecular H-bonding, and (d) π–π stacking interaction.
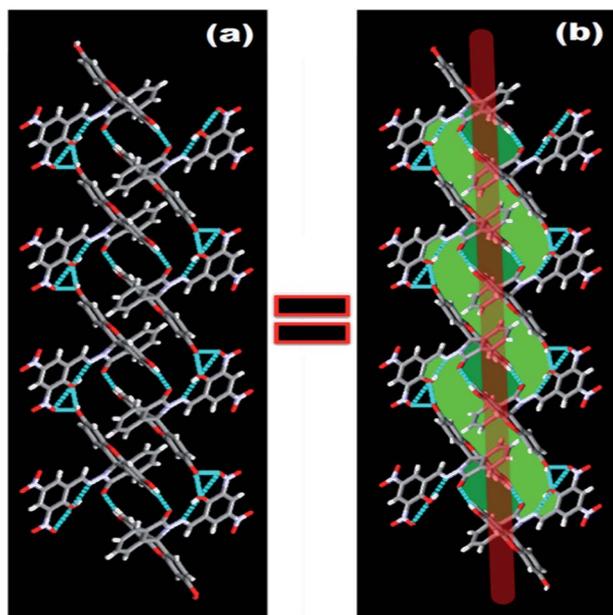
Fig. 3 The packing of **FDNS** along *b* axis (a) and corresponding double helical structure (b).

molecule with a hydroxyl group (H003···O7) of other **FDNS**. A weaker aromatic stacking interaction between xanthene moieties of two **FDNS** molecules also occur at interplanar separation of 4.25 Å as depicted in (Fig. 2d). The hydrogen bondings played significant role in the construction of supramolecular architecture propagating along different crystallographic axes. The packing structure of **FDNS** shows three different structures along three different axes. Along '*a*' axis, it looks like a series of incandescent body connected *via* a single wire (Fig. S5†), whereas along '*b*' as a double helical structure (Fig. 3) and along '*c*' axis as a H-shaped structure (Fig. S6†).

3.1. Spectral recognition of Cu^{2+} and Hg^{2+} by FDNS

Binding of several cations with **FDNS** were checked by adding their excess solution (10.0 eq.) separately to a solution of **FDNS** (10^{-5} M, aqueous : MeOH, 8 : 2 v/v, HEPES buffer (1 mM), pH 7.4) (Fig. S7†). On addition of a fixed amount (10.0 equiv.) of Cu^{2+} ions to the **FDNS**, a momentous enrichment in absorbance at $\lambda_{max} = 495$ nm was observed with a concomitant disappearance of the band at $\lambda_{max} = 401$ nm. It induces a clear colour change of **FDNS** solution from a yellow to light brown. However, the addition of other competitive metal ions (Li^+, Hg^{2+}, Ca^{2+}, Cd^{2+}, Fe^{3+}, Na^+, Al^{3+}, Zn^{2+}, Pb^{2+}, Mg^{2+}, Cu^{2+}, Co^{2+}, Ni^{2+}, and Ag^+ ions) did not show any considerable colour change and spectral variation under the same conditions. It suggested a high selectivity of **FDNS** toward Cu^{2+} ions (Fig. S8†). The fluorescence response of **FDNS** with different cations was also studied as depicted in Fig. S9.† The non fluorescent **FDNS** did not show any distinct change in its emission pattern on the addition Cu^{2+} ions. However, under the similar condition, a passionate fluorescence enhancement in presence of excess Hg^{2+} ions was observed with a peak at $\lambda_{em} = 517$ nm. It could be ascribed to

the combinatorial effect of ring opening of **FDNS** and chelation of Hg^{2+} ions to it. The spectral pattern remains unbothered on the addition of several other competing metal ions.

3.2. Spectral titrations

The spectrophotometric titrations were performed to analyse the interaction of **FDNS** with Cu^{2+} ions at 25 °C in aqueous : MeOH (8 : 2 v/v, HEPES buffer(1 mM), pH 7.4). As shown in Fig. 4, a new absorption band centred at $\lambda_{max} = 495$ nm gradually arises on the incremental addition of Cu^{2+} (0–1 equiv.) with concomitant change in the colour from yellow to light brown (inset of Fig. 4). An isobestic point is observed at $\lambda_{max} = 382$ and 448 nm. The stoichiometric affiliation between **FDNS** and Cu^{2+} was found to be 1 : 1 based on the change in absorbance at $\lambda_{max} = 495$ nm. The fluorescent spectra as shown in Fig. 5, were obtained on excitation at $\lambda_{ex} = 495$ nm.

Free **FDNS** was found weak-fluorescent. However, on incremental addition of Hg^{2+} ions to **FDNS** solution, a strong fluorescence with a band centred at $\lambda_{em} = 517$ nm was displayed. It was attributed to chelation enhanced fluorescence (CHEF) effect.[28–30] The change in colour under UV light occurs as depicted in inset of Fig. 5. Thus, **FDNS** has very alluring "turn-on" fluorescence selectivity, for detection of toxic Hg^{2+} ions.[31–36] **FDNS** remains non fluorescent on the addition of Cu^{2+} ions owing to paramagnetic effect arising from spin–orbit coupling of the Cu^{2+} ions.[36] Moreover, in case of absorbance, addition of Cu^{2+} ions followed an exponential increase (Fig. S10†) while in case of fluorescence, there is a linear increase on incremental addition of Hg^{2+} ions (Fig. S11†). The binding constant for Cu^{2+} and Hg^{2+} at $R^2 = 0.99$, computed using the Benesi–Hildebrand method are found as 2.55×10^5 and 4.79×10^4 M^{-1} respectively. The corresponding graphs are shown in Fig. S12 and S13,† respectively. The maximum point at 0.5 for Cu^{2+} and Hg^{2+} in Job's plots also indicated that **FDNS** formed 1 : 1 complexes with Cu^{2+} and Hg^{2+} (Fig. S14 and S15†). The detection limit of

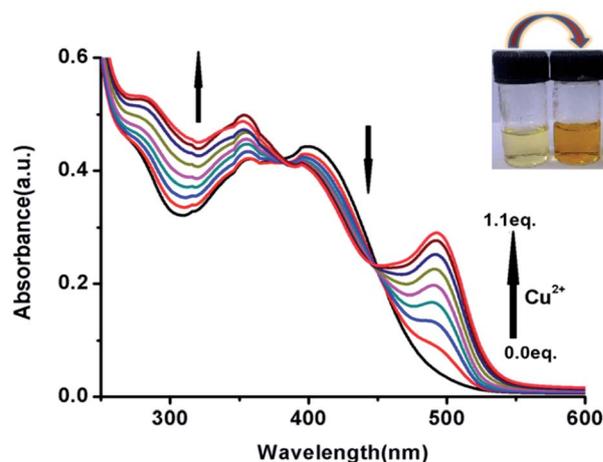**Fig. 4** Absorption spectral titrations of **FDNS** (10 μM) in aqueous : MeOH (8 : 2 v/v) HEPES buffer (1 mM, pH 7.4) on the incremental addition of aqueous solution of $Cu(NO_3)_2$ (1.1 equiv.). Inset: visual change in the colour of **FDNS** solution in the presence of Cu^{2+} ions under normal light.
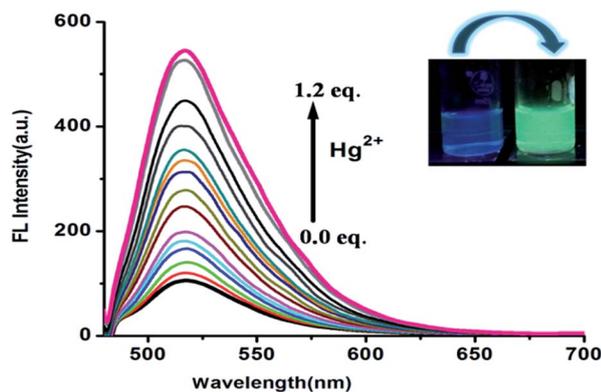
Fig. 5 Fluorescence spectral titrations of **FDNS** (10 μM) in aqueous : MeOH (8 : 2 v/v) HEPES buffer (1 mM, pH 7.4) on the incremental addition of $Hg(NO_3)_2$ (1.2 equiv.) λ_{ex} = 465 nm. Inset: the colour change of **FDNS** solution in the presence of Hg^{2+} ions under UV light.

FDNS for Cu^{2+} and Hg^{2+} was found as 4.13×10^{-7} M and 2.50×10^{-7} M respectively, (Fig. S16 and S17†). It suggested that **FDNS** is an efficient system for monitoring traces of Cu^{2+} and Hg^{2+} ions. Thus, present probe turned out to be a multiple ion sensor exploiting both chromogenic and fluorogenic applications with a better detection limit as compared to earlier reported probe.[22] Additionally, among several reported colorimetric probes,[37] the present probe again turned out to be comparable with the detection limit and also in some case with stronger binding of Cu^{2+} ions.[38] The quantum yield of **FDNS** (0.035) is enhanced upon binding with the Hg^{2+} ions (0.095) using fluorescein as a standard (0.5 in ethanol). However, some of the fluorescent probe reported earlier[39] could not enhance the quantum yield on binding of Hg^{2+} ions. Thus, **FDNS** again turned out to be sensitive probe for Hg^{2+} ions.

3.3. Selectivity of FDNS to Cu^{2+} and Hg^{2+} ions

It is challenging to achieve selectivity of specific analyte over competing species in the area of the development of sensors. To appraise the selectivity of **FDNS** for Cu^{2+} and Hg^{2+} ions in reality, competition experiments were also carried out. **FDNS** was added separately to a solution of Cu^{2+} and Hg^{2+} ions in the existence of other cations, such as Li^+, Ca^{2+}, Cd^{2+}, Cr^{3+}, Fe^{3+}, K^+, Na^+, Al^{3+}, Zn^{2+}, Pb^{2+}, Mg^{2+}, Co^{2+}, Ni^{2+}, Ag^+. As shown in Fig. S18,† for detection of Cu^{2+} ions, these ions did not reveal any noticeable interference in the absorption spectrum. Similarly, for detection of Hg^{2+} ions no significant interference was observed in the emission spectrum (Fig. S19†).

3.4. Reversibility of FDNS for sensing Cu^{2+} and Hg^{2+}

Reversibility is significant parameter to check the practicability of a sensor. To realize the reversibility of the proposed **FDNS**–Cu^{2+} and **FHY**–Hg^{2+} species, EDTA and S^{2-} addition experiments were performed in the aqueous : MeOH solution, respectively. It was found that on addition of 2 equiv. EDTA solution to **FDNS**–Cu^{2+} adduct the absorbance decreased completely and reappears on further addition of Cu^{2+} ions
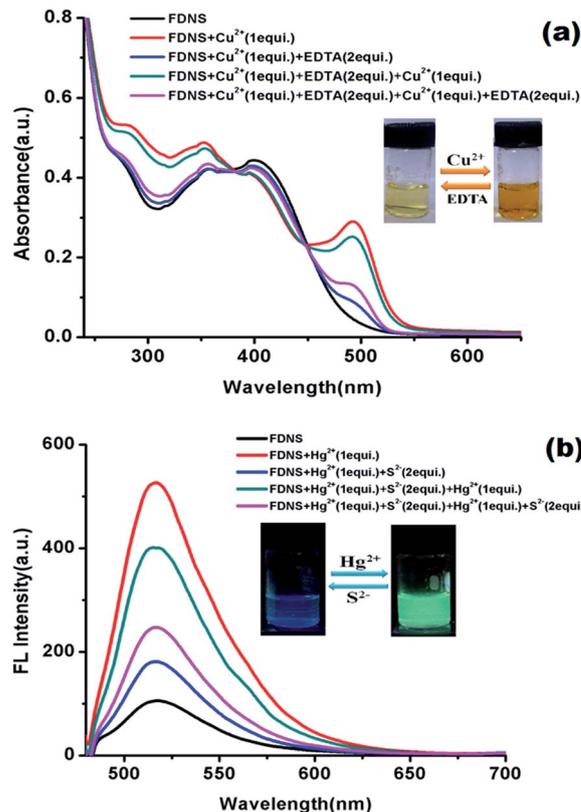

Fig. 6 Reversibility of **FDNS** evaluated by the alternative additions of (a) Cu^{2+} and EDTA (EDTA is 2 equiv. to Cu^{2+}) alternately to the **FDNS** solution. Inset: visual change in the colour of **FDNS** solution in the presence of Cu^{2+} and EDTA under normal light and (b) Hg^{2+} and S^{2-} ions (S^{2-} is 2 equiv. to Hg^{2+}) alternately to the **FDNS** solution. Inset: the colour change of **FDNS** solution in the presence of Hg^{2+} and S^{2-} ions under UV light.

(Fig. 6a). It was repeated to six cycles (Fig. S20†). Similarly, the response of **FHY**–Hg^{2+} adduct with Na_2S was found reversible. After adding specific concentration of Na_2S (2 equiv.), fluorescence intensity was quenched (Fig. 6b) which was almost completely recovered on further addition of Hg^{2+} ions. This restoration capability indicates that **FDNS** could be re-used with suitable management.

It was interesting to observe a clear change in colour from brown to green on addition of tetrabutylammonium cyanide solution to **FDNS**–Cu^{2+} adduct, which finally change into red colour solution (Fig. S21†). In due course of time (72 h), red coloured crystals of a new compound (**FKCN**) were obtained. It was characterized using spectroscopic (IR, ^1H, ^{13}C NMR) and X-ray crystallography. It was observed that the tetrabutylammonium cation was co-crystallized with **FDNS**. The molecular structure (ORTEP diagram) of **FKCN** is depicted in Fig. 7 and its structural refinement parameters are given in Table S1.† IR spectrum of **FKCN** displays a distinct peak at ν 1603 cm^{-1} assigned to ν(HC=N) vibration (Fig. S22†). ^1H spectrum (Fig. S23†) of **FKCN** further confirms the existence of CH=N proton at δ 8.81 ppm. Its ^{13}C NMR spectrum (Fig. S24†) showed a peak at δ 64.84 ppm and supports the presence of spiro carbon
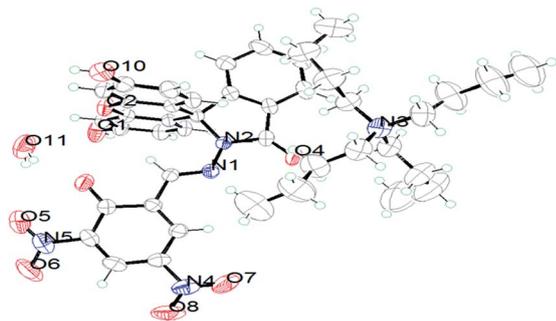
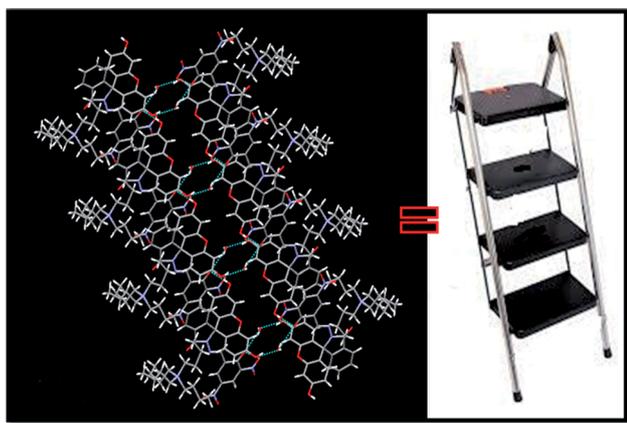**Fig. 7** Molecular structure (ORTEP) of **FKCN** at 40% probability level.

Fig. 8 Intermolecular hydrogen bonds between two molecules of **FKCN** via co-crystallised water molecule showing the formation of ladder structure.

in its structure. The UV-visible spectrum of **FKCN** showed peaks at $\lambda_{max} = 399$ nm ($\varepsilon = 26\,600$ M^{-1} cm^{-1}) assigned to intra-molecular charge transfer transition. It crystallizes in a triclinic crystal system with $P\bar{1}$ space group. In **FKCN**, dihedral angle between spirolactam and xanthene plane is found as 89.64(2)° as depicted in Fig. S25.†

Intermolecular hydrogen bonds between two molecules of **FKCN** via co-crystallised water molecule O11–H1w···O3, O10–H10···O11 stabilizes the crystal structure and forms supramolecular structure with cavity (Fig. S26†) while incorporation of another intermolecular hydrogen bonding of type O1–H010···O3 between hydroxyl group (O1–H010) of a **FKCN** to carbonyl group of another neighbouring **FKCN** forms ladder like structure (Fig. 8).

3.5. Probable mechanism of recognition of cations

IR spectrum (Fig. S27†) of a solid isolated by the addition of Cu^{2+} ions to **FDNS**, showed major peaks at 1614.58 and 1645.8 cm^{-1}. These peaks were assigned to ν(CH=N) and ν(C=O) respectively and shifted significantly as compared to peak observed for free **FDNS**. It supported that both groups of **FDNS** had coordinated with Cu^{2+} ion. The ESI-MS data of this adduct displayed a peak at m/z 639.0066 (Fig. S28†) which corresponds to the parent ion as [**FDNS** + Cu^{2+} + 2H$_2$O] + 1. It further
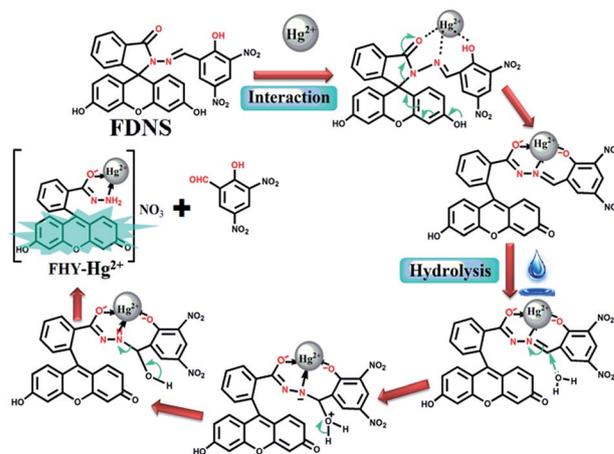
Scheme 2 Plausible mechanism for interaction of **FDNS** with Cu^{2+} ions and tetrabutylammonium cyanide.

supported the formation of a 1 : 1 copper adduct as evidenced from the absorption titrations.[40,41] The isolation of **FKCN** supported that **FDNS**–Cu^{2+} adduct interact with tetrabutylammonium cyanide via displacement approach as shown in Scheme 2. The binding of **FDNS** with Hg^{2+} ions was substantiated by its ^{1}H NMR titrations in a mixture of DMSO-d$_6$ and D$_2$O. As shown in Fig. S29,† on the incremental addition of Hg^{2+}, the imine proton (CH=N) shifted from δ 9.03 to 9.23 ppm. It supported the coordination of Hg^{2+} to **FDNS**. The phenolic proton (OH) of **FDNS** also moved to downfield by $\delta = 0.29$ ppm (9.93 to 10.12 ppm) and finally disappeared. Interestingly, a new peak emerged at $\delta = 10.42$ ppm. It was assigned to an aldehyde proton. The above data imply that Hg^{2+} ion may first coordinated to the **FDNS** and then results in its hydrolysis. The ESI-MS of solid thus obtained gave a peak at $m/z = 544.4615$ (Fig. S30†). It supported the formation of fluorescein hydrazide (**FHY**)–Hg^{2+} adduct,[42–44] further supported by its IR spectrum (Fig. S31†). Thus, based on these observations, a tentative mechanism of binding of Hg^{2+} ions to **FDNS** is proposed as shown in Scheme 3.
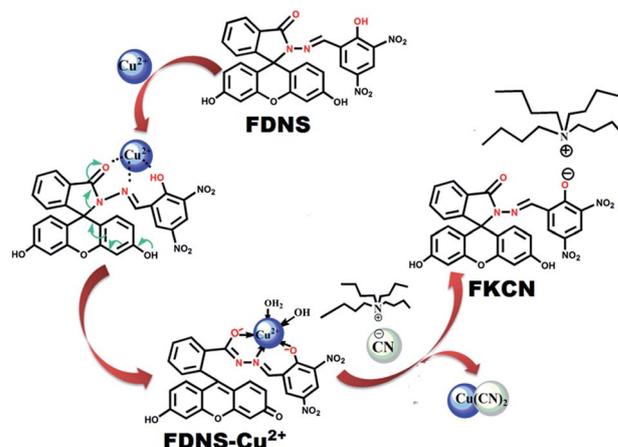
Scheme 3 Plausible mechanism for interaction of **FDNS** with Hg^{2+} ions.

3.6. pH effects on sensing by FDNS

To check the sensing ability of **FDNS** at physiological level, pH effect of free **FDNS** and **FDNS**–Cu^{2+}/Hg^{2+} adducts on the absorption and emission spectra were recorded over a wider range of pH (2.0–12.0). It was observed that the solution of **FDNS** showed insignificant absorption and emission in pH range 2.0–6.0; signifying that the **FDNS** was stable over this pH range.[45] But as depicted in Fig. S32(a),† an intense absorption was observed after Cu^{2+} ions addition to **FDNS** solution. (pH 7.0 or more.)

Similarly, the fluorescence intensity of **FHY**–Hg^{2+} assembly also increases in the region of pH 7.0–12.0 as depicted in Fig. S32(b).† Thus, the response behaviour of **FDNS** separately to Cu^{2+} and Hg^{2+} ions could be studied under physiological conditions.

3.7. Time-dependence detection process of Cu^{2+} and Hg^{2+}

The reaction time profile of **FDNS** separately with Cu^{2+} and Hg^{2+} ions are also studied. The kinetics of the reaction was complete within 40 and 25 seconds for Cu^{2+} and Hg^{2+} respectively. It showed that this probe react very rapidly with selective ions under the experimental conditions as shown in Fig. S33(a) and S33(b),† respectively.

3.8. Sequential logic gate operations

Sequential circuits useful for the memory devices, function *via* feedback loop where one of the output obtained is used as the input and recognised as the 'memory element'.[46] Thus, a sequential logic circuit is designed on the basis of Cu^{2+} and EDTA as chemical inputs which are designated as input A and input B. The absorption at $\lambda_{max} = 495$ nm and visual detection are considered as OUT1 and OUT2, respectively. A value of 0.12 was calculated as threshold value of OUT1 as depicted in Fig. S34.† A logic circuit having two inputs (input A and input B) and two outputs have been constructed and the concerned truth table is shown in Fig. 9. Furthermore, the switchability of **FDNS** controlled by Hg^{2+} and S^{2-} also commune information as two inputs and two outputs. The fluorescence signal at 517 nm functions as output 1 and the colour change of **FDNS** after addition of Hg^{2+} in UV light as output 2 and corresponding sequential logic circuits are depicted in Fig. S35 and S36.† A value of 200 as threshold value was fixed as OUT1 at $\lambda_{em} =$
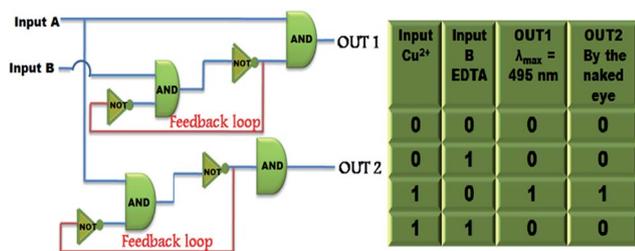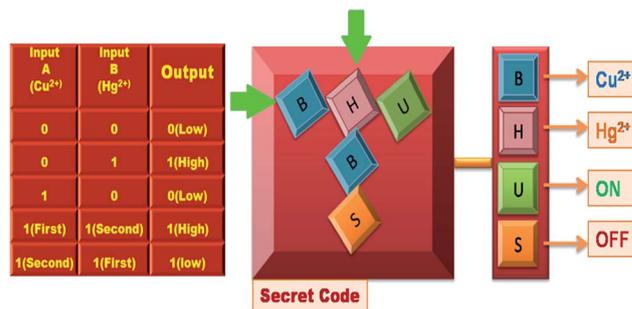

Fig. 10 Schematic representation of keypad locks and truth table of lock to access a secret code by observing the fluorescence at 517 nm with different inputs.

517 nm for the fluorescence intensity. '1' is denoted for the fluorescence intensity greater than threshold value and '0' is represented for the intensity lower than the threshold value which corresponds to the 'ON' and 'OFF' states of the readout signals.

This system is also utilized for the construction of a security keypad lock depending on the sequential addition of Cu^{2+} and Hg^{2+} as inputs **1** and **2** respectively (Fig. S37†). The receptor **FDNS** shows no significant emission band at 517 nm in the absence of any chemical input hence output is 0 (OFF-state). The addition of Cu^{2+} to **FDNS** gives the output '0' (OFF-state) but it is reversed to '1' (ON-state) with the chronological addition of another input Hg^{2+}. However, on changing the input sequence, Hg^{2+} as the first input with subsequent addition of Cu^{2+} as second input, the fluorescence intensity is observed below its threshold limit, thus output is represented as zero. Inputs Cu^{2+} and Hg^{2+} were represented as 'B' and 'H' respectively. There are two possibilities of inputs sequence: (a) addition of 'B' followed by 'H' where the receptor **FDNS** causes emission above threshold limit at λ_{em} 517 nm and this 'ON' state is assigned by 'U' which generate a secret code 'BHU'. In the reverse sequence, 'H' is followed by 'B', the fluorescence at 517 nm get quenched which is 'OFF' state and is denoted by 'S'. This sequence (HBS) failed to open the keypad lock. Hence, for the construction of the molecular keypad lock, 'BHU', inputs in specific sequence is essential. The schematic representation of keypad lock with corresponding truth table is depicted in Fig. 10.

More than 700 different combinations are observed by the use of numerical digits (0–9) and letters (A–Z) as 'PIN' in a two-digit password.[47] Thus, unlocking the keypad lock becomes more complex which substantially enhances the security of the devices at molecular level. Thus, keypad lock can be unlocked only by the users who know the correct passwords.

3.9. Role of FDNS in the analysis of Cu^{2+} and Hg^{2+} ions in water samples

The role of **FDNS** for analysis of Cu^{2+} and Hg^{2+} ions in natural water were done by using proof-of-concept experiments without any prior sanitization.[48] Three water sample were collected from the different sources such as River Ganga (Assi), pond

Fig. 9 Truth table and sequential logic circuits displaying memory units with two inputs (input A (Cu^{2+}) and input B (EDTA)) and two outputs in the presence of chemical inputs.

(Durgakund) and lake (Motijheel), all from Varanasi City, India. The solution of Hg(NO$_3$)$_2$ (0–10 μM) were spiked into these samples followed by addition of **FDNS** (10 μM). A good linear curve was obtained between fluorescence intensity *versus* concentration of Hg^{2+} in the range of 2–10 μM (Fig. S38†). This clearly shows the potential relevance of **FDNS** for detection of Hg^{2+} ions in ecological water (Table S4†). Similarly, nitrate salt of Cu^{2+} ions (0–10 μM) were spiked into the water samples solution followed by the addition of **FDNS** (10 μM). Here also a linear graph between the absorption and the Cu^{2+} ion concentration in the range of 2–8 μM (Fig. S39†). The data are presented Table S5.† The experimental results suggested **FDNS** is relevant for effective analysis of Cu^{2+} or Hg^{2+} ions in natural water sources.

3.10. Fast track detection of Cu^{2+} and Hg^{2+} ions

To ensure the cleanliness of the drinking water and consumable food stuffs in remote places is a great challenge now days. Therefore, for on-site detection of Cu^{2+} and Hg^{2+} ions a manageable test strips were equipped, as they did not need any complicated equipments. Since, for this filter-paper strips were first soaked in **FDNS** solution and then air dried. After that filter-paper dipped in a Cu^{2+} solution (1 equiv.). A distinct visible light brown colour change was observed immediately as shown in Fig. 11a. The test-strips change its colour to fluorescent green under UV light in the presence of Hg^{2+} ion only (Fig. 11b). This makes the probes pretty useful for quick on-site detection of metal ions in real samples.[49]

3.11. Live cell imaging of FDNS and detection of Hg^{2+} ions in cervical cancer cell lines

The uptake of **FDNS** by ME-180 cervical cancer cells is detected by fluorescence microscopy. **FDNS** treated live cells showed green fluorescence throughout the cells while control treated with solvent has no fluorescence (Fig. 12A and B).

Interestingly, **FDNS** mediated fluorescence was enhanced about 1.5 folds upon the addition of mercury (Hg^{2+}) (Fig. 12C). Magnified bright field images as depicted in Fig. 12D–F showed that cells are intact. The Fig. 12H and I show that compound is distributed throughout the cell and their intensity graph is
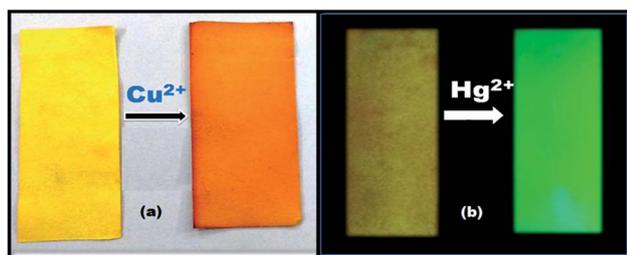

Fig. 11 (a) Naked eye detection on a piece of paper soaked with **FDNS**: from left to right **FDNS** (blank); **FDNS** + Cu^{2+} (b) the variation of the color of **FDNS** coated on filter paper before (left) and after treatment with Hg^{2+} (right) under UV excitation light.
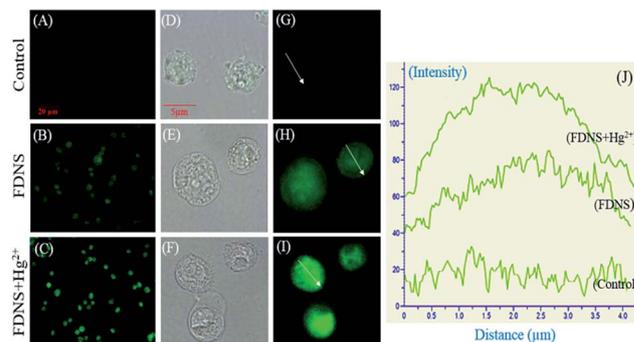

Fig. 12 Fluorescence images of ME-180 cervical cancer cells. (A) Control-cells (B) cells treated with 10 μM **FDNS** and (C) **FDNS** treated cells in presence of 50 μM Hg^{2+}. Magnified bright field images (D–F) show intact ME-180 cells and their respective fluorescence images (G–I) show the presence of compound throughout the cells. Intensity graph (J) of cells (white-arrow) show relative fluorescence intensity for respective set of experiments. Scale bar in panel A–C is 20 μm while 5 μm in D–I.

depicted in Fig. 12J. Hence, compound **FDNS** has wider permeability in ME-180 cervical cancer cells.

4. Conclusions

In summary, fluorescein hydrazone **FDNS** is synthesized by the condensation of 3,5-dinitrosalicylaldehyde with fluorescein hydrazide. It is effectively characterized using spectroscopic techniques and further supported by its X-ray crystallography. This molecule empowers the formation of interesting supramolecular structures *via* intermolecular H-bonding. **FDNS** exhibits a colorimetric response to Cu^{2+} ions with naked eye visibility followed by spectral titrations without any interference from several relevant metal ions. The addition of a solution of tetrabutylammoniumcyanide in methanol to a corresponding solution of **FDNS**–Cu^{2+} ensemble enables it as a secondary sensor of CN$^-$ ions and provides a novel organic compounds **FKCN** containing deprotonated **FDNS** co-crystallized with tetrabutylammonium cation. The Hg^{2+} and Cu^{2+} are selectively detected in the presence of several other metal ions with a detection limits of 4.13 × 10^{-7} M and 2.50 × 10^{-7} M, respectively. The sensing mechanisms of **FDNS** for Cu^{2+} ions follows opening of spirolactam ring on its binding to **FDNS**. However, binding of Hg^{2+} ions to **FDNS** leads hydrolysis of CH=N group bringing "turn on" fluorescence. The other potential applications of **FDNS** involves its uses as memory device, paper strip tests for the analysis of Cu^{2+} and Hg^{2+} ions in the contaminated samples. The live cell imaging also promotes its application in real world.

Acknowledgements

References

1 A. Ajaya ghosh, P. Carol and S. Sreejith, *J. Am. Chem. Soc.*, 2005, **127**, 14962.

2 J. W. Lee, H. S. Jung, P. S. Kwon, J. W. Kim, R. A. Bartsch, Y. Kim, S. Kim and J. S. Kim, *Org. Lett.*, 2008, **10**, 3801.

3 L. Xue, Q. Liu and H. Jiang, *Org. Lett.*, 2009, **11**, 3454.

4 M. Leermakers, W. Baeyens, P. Quevauviller and M. Horvat, *Trends Anal. Chem.*, 2005, **24**, 383.

5 C. C. Huang and H. T. Chang, *Anal. Chem.*, 2006, **78**, 8332.

6 S. Cai, Y. Lu, S. He, F. Wei, L. Zhao and X. Zeng, *Chem. Commun.*, 2013, **49**, 822.

7 T. Hirano, K. Kikuchi, Y. Urano, T. Higuchi and T. Nagano, *J. Am. Chem. Soc.*, 2000, **122**, 12399.

8 G. K. Walkup, S. C. Burdette, S. J. Lippard and R. Y. Tsien, *J. Am. Chem. Soc.*, 2000, **122**, 5644.

9 T. Hirano, K. Kikuchi, Y. Urano, T. Higushi and T. Nagano, *Angew. Chem., Int. Ed.*, 2000, **39**, 1052.

10 S. C. Burdette, G. K. Walkup, B. Spingler, R. Y. Tsien and S. J. Lippard, *J. Am. Chem. Soc.*, 2001, **123**, 7831.

11 K. R. Gee, Z. L. Zhou, W. J. Qian and R. Kennedy, *J. Am. Chem. Soc.*, 2002, **124**, 776.

12 S. C. Burdette, C. J. Frederickson, W. Bu and S. J. Lippard, *J. Am. Chem. Soc.*, 2003, **125**, 1778.

13 M. Suresh, A. Ghosh and A. Das, *Chem. Commun.*, 2008, **44**, 3906.

14 W. J. Shi, J. Y. Liu and D. K. P. Ng, *Chem.–Asian J.*, 2012, **7**, 196.

15 K. J. Barnham, C. L. Masters and A. I. Bush, *Nat. Rev. Drug Discovery*, 2004, **3**, 205.

16 E. Gaggelli, H. Kozlowski, D. Valensin and G. Valensin, *Chem. Rev.*, 2006, **106**, 1995.

17 X. Zeng, L. Dong, C. Wu, L. Mu, S. F. Xue and Z. Tao, *Sens. Actuators, B*, 2009, **141**, 506.

18 L. Tang, F. Li, M. Liu and R. Nandhakumar, *Spectrochim. Acta, Part A*, 2011, **78**, 1168.

19 N. Sharma, S. I. Reja, V. Bhalla and M. Kumar, *Dalton Trans.*, 2014, **43**, 15929.

20 H. Y. Lee, K. M. K. Swamy, J. Y. Jung, G. Kim and J. Yoon, *Sens. Actuators, B*, 2013, **182**, 530.

21 R. Prajapati, L. Mishra, S. J. Grabwoski, G. Govil and S. K. Dubey, *J. Mol. Struct.*, 2008, **879**, 1.

22 Y. Yang, F. Huo, C. Yin, Y. Chu, J. Chao, Y. Zhang, J. Zhang, S. Li, H. Lv, A. Zheng and D. Liu, *Sens. Actuators, B*, 2013, **177**, 1189.

23 G. M. Sheldrick, *SHELXS-97 Program for the Solution of Crystal Structures*, University of Göttingen, Göttingen, Germany, 1997.

24 G. M. Sheldrick, Phase annealing in SHELX-90, *Acta Crystallogr., Sect. A: Found. Crystallogr.*, 1990, **46**, 467.

25 H. A. Benesi and J. H. Hildebrand, *J. Am. Chem. Soc.*, 1949, **71**, 2703.

26 A. Hakonen Plasmon, *Anal. Chem.*, 2009, **81**, 4555.

27 D. Wang, X. Xiang, X. Yang, X. Wang, Y. Guo, W. Liu and W. Qin, *Sens. Actuators, B*, 2014, **201**, 246.

28 E. M. Nolan and S. J. Lippard, *Chem. Rev.*, 2008, **108**, 3443.

29 A. Tamayo, B. Pedras, C. Lodeiro, L. Escriche, J. Casabo, L. Capelo, B. Covelo, R. Kiveka and R. Sillanpa, *Inorg. Chem.*, 2007, **46**, 159.

30 Y. Zhang, Y. Yang, J. Hao, C. Yin, F. Huo, J. Chao and D. Liu, *Spectrochim. Acta, Part A*, 2014, **132**, 27.

31 Y. Yang, K. Yook and J. Tae, *J. Am. Chem. Soc.*, 2005, **1**, 16760.

32 G. Zhang, D. Zhang, S. Yin, X. Yang, Z. Shuai and D. Zhu, *Chem. Commun.*, 2005, **6**, 2161.

33 X. Guo, X. Qian and L. Jia, *J. Am. Chem. Soc.*, 2004, **126**, 2272.

34 G. Hennrich, W. Walther, U. Resch-genger and H. Sonnenschein, *Inorg. Chem.*, 2001, **40**, 641.

35 Y. Zhao, Z. Lin, C. He, H. Wu and C. Duan, *Inorg. Chem.*, 2006, **45**, 10013.

36 A. P. De Silva, H. Q. N. Gunarante, T. Gunnlaugsson, A. J. M. Huxley, C. P. McCoy, J. T. Rademacher and T. E. Rice, *Chem. Rev.*, 1997, **97**, 1515.

37 X. Wu, X. Gong, W. Dong, J. Ma, J. Chao, C. Li, L. Wang and C. Dong, *RSC Adv.*, 2016, **6**, 59677 and references therein.

38 H. M. Chawla, R. Shukla and S. Pandey, *Tetrahedron Lett.*, 2013, **54**, 2063.

39 E. M. Nolan, M. E. Racine and S. J. Lippard, *Inorg. Chem.*, 2006, **45**, 2742.

40 Z. Q. Guo, W. H. Zhu, L. J. Shen and H. Tian, *Angew. Chem.*, 2007, **119**, 5645.

41 J. Mao, L. N. Wang, W. Dou, X. L. Tang, Y. Yan and W. S. Liu, *Org. Lett.*, 2007, **9**, 4567.

42 H. Cheng and Y. Qian, *RSC Adv.*, 2015, **5**, 82887.

43 H. A. Benesi and J. H. Hildebrand, *J. Am. Chem. Soc.*, 1949, **71**, 2703.

44 S. Tatay, P. Gavin, E. Coronado and E. Palomares, *Org. Lett.*, 2006, **8**, 3857.

45 E. M. Nolan and S. J. Lippard, *J. Am. Chem. Soc.*, 2003, **125**, 14270.

46 T. Mistri, R. Alam, R. Bhowmick, A. Katarkar, K. Chaudhuri and M. Ali, *New J. Chem.*, 2016, **40**, 330.

47 M. Suresh, A. Ghosh and A. Das, *Chem. Commun.*, 2008, 3906.

48 H. L. Li, J. L. Fan, F. L. Song, H. Zhu, J. J. Du, S. G. Sun and X. J. Peng, *Chem.–Eur. J.*, 2010, **16**, 12349.

49 L. D. Chebrolu, S. Thurakkal, H. S. Balaraman and R. Danaboyina, *Sens. Actuators, B*, 2014, **8**, 204.